

Structural and Thermal Properties of the Tetragonal Cobalt Manganese Spinel $Mn_xCo_{3-x}O_4$ ($1.4 < x < 2.0$)

Eladio Vila, Rosa M. Rojas,* José L. Martín de Vidales,[†] and Oscar García-Martínez

Instituto de Ciencia de Materiales de Madrid, CSIC, Cantoblanco, 28049 Madrid, Spain

Received October 24, 1995. Revised Manuscript Received February 15, 1996[®]

Phase transitions experienced by $Mn_xCo_{3-x}O_4$ ($1.4 < x < 2.0$) materials synthesized at low temperature have been followed by X-ray powder diffraction and thermal analysis. A tetragonal single phase (space group $I41/amd$) has been isolated for the first time for samples quenched from $T > 700$ °C, with a distortion parameter ranging from 1.0263(1) for $x = 1.45$ to 1.1353(1) for $x = 1.9$. The existence at $T > 725$ °C of a nonisolable cubic spinel single phase (space group $Fd\bar{3}m$) in the whole compositional range has been shown by high-temperature X-ray diffraction techniques. It readily transforms on quenching into the new tetragonal single phase. When the cubic high-temperature single phase is allowed to cool slowly, it decomposes into a mixture of tetragonal ($x \approx 2$) and cubic ($x \approx 1.3$) spinel-type phases. The composition $x = 1.4$ is found to be the upper compositional limit of existence of the cubic $Fd\bar{3}m$ spinel, when it is synthesized by a low-temperature procedure.

Introduction

Cobalt manganese spinel-type oxides constitute a group of materials that have been widely studied by many investigators. They have been systematically studied with regard to several topics: (i) influence of the synthesis conditions on the oxidation states and cation distribution^{1–6} in the cubic and tetragonal phases “traditionally” described in the Co–Mn–O system;^{7–9} (ii) physical and chemical properties such as catalytic activity,^{6,10} and more recently (iii) the potential applications of $Mn_xCo_{3-x}O_4$ as precursors in the preparation of the λ - MnO_2 cathode material.¹¹

Spinel-like materials are rather sensitive to the synthesis conditions, which can affect morphological and structural properties. In some foregoing papers we have reported about the synthesis at low temperature of cobalt manganese oxides $Mn_xCo_{3-x}O_4$.^{11–13} The procedure, based on the coprecipitation with 1 M *n*-butylamine at pH \approx 10.5, of stoichiometric aqueous solutions of cobalt and manganese chlorides, yielded highly reac-

tive materials and allowed the formation at 200 °C of a cubic form (space group $Fd\bar{3}m$) between $0 \leq x \leq 1.4$, in contrast with the upper limits of 1.2¹⁴ or 1.3³ for the cubic $Fd\bar{3}m$ spinel-like phase synthesized by the ceramic procedure, or from thermal decomposition of mixed carbonate precursors.¹⁵ For compositions $2 \leq x \leq 3$ the oxides crystallize with the tetragonal $I41/amd$ spinel-type structure, as has been already reported.^{1,4,6,16,17}

Materials $Mn_xCo_{3-x}O_4$ ($1.4 < x < 2.0$) obtained at 200 °C are mixtures of cubic and tetragonal spinel-type phases. However, if they are quenched from 700 °C, the formation of a tetragonal $I41/amd$ single phase is achieved.¹¹ Therefore, three well-defined solid solutions in the Mn–Co–O system have been established and their fields of existence delimited.¹¹ For cubic $Mn_xCo_{3-x}O_4$ ($0 \leq x \leq 1.4$), the cell parameter linearly increases from 8.0769(2) for Co_3O_4 ($x = 0$) to 8.3216(3) Å ($x = 1.4$). The cell dimensions of the tetragonal phase formed between $2 \leq x \leq 3$ show the same trend; *a* goes from 5.7296(6) to 5.7561(2) Å, while *c* varies from 9.2304(9) to 9.4599(2) Å, with distortion parameter c/a' ($a' = \sqrt{2}a$) ranging from 1.139 to 1.162.

Considering the high reactivity of the spinel oxides synthesized by the low-temperature procedure and the influence of the structure on the physicochemical properties of these materials, this paper concerns the structural features and the evolution with temperature of the new tetragonal spinel-like single phases formed in the compositional range $Mn_xCo_{3-x}O_4$ ($1.4 < x < 2.0$). A careful characterization of the oxide with composition $x = 1.4$, corresponding to the new established upper limit for the cubic $Fd\bar{3}m$ phase, has also been carried out. These results can contribute to a better definition of the Co–Mn–O phase diagram.

[†] Facultad de Ciencias (C-VI), U.A.M., Cantoblanco, 28049 Madrid, Spain.

[®] Abstract published in *Advance ACS Abstracts*, April 1, 1996.

- (1) Buhl, R. *J. Phys. Chem. Solids* **1969**, *30*, 805.
- (2) Boucher, B.; Buhl, R.; di Bella, R.; Perrin, M. *J. Phys.* **1970**, *31*, 113.
- (3) Naka, S.; Inagaki, M.; Tanaka, T. *J. Mater. Sci.* **1972**, *7*, 441.
- (4) Yamamoto, N.; Kawano, S.; Achiwa, N.; Higashi, S. *J. Jpn. Soc. Powder Metall.* **1983**, *30*, 48.
- (5) Yamamoto, N.; Higashi, S.; Kawano, S.; Achiwa, N. *J. Mat. Sci. Lett.* **1983**, *2*, 525.
- (6) Wright, P. A.; Natarajan, S.; Thomas, J. M.; Gai-Boyes, P. L. *Chem. Mater.* **1992**, *4*, 1053.
- (7) Aukrust, E.; Muan, A. *J. Am. Ceram. Soc.* **1963**, *46*, 511.
- (8) Golikov, Yu. V.; Tubin, S. Ya.; Barkhatov V. P.; Balakirev, V. F. *Phys. Chem. Solids* **1985**, *46*, 539.
- (9) Golikov, Yu. V. *Inorg. Mater.* **1988**, *24*, 975.
- (10) Yang, B. L.; Chan, S. F.; Chang, W. S.; Chen, Y. Z. *J. Catal.* **1991**, *130*, 52.
- (11) Martín de Vidales, J. L.; Vila, E.; Rojas, R. M.; García-Martínez, O. *Chem. Mater.* **1995**, *7*, 1716.
- (12) Martín de Vidales, J. L.; García-Martínez, O.; Vila, E.; Rojas, R. M.; Torralvo, M. J. *Mater. Res. Bull.* **1993**, *28*, 1135.
- (13) Rojas, R. M.; Vila, E.; García-Martínez, O.; Martín de Vidales, J. L. *J. Mater. Chem.* **1994**, *4*, 1635.

(14) Wickham, D. G.; Croft, W. J. *J. Phys. Chem. Solids* **1958**, *7*, 351.

(15) Jimenez-Mateo, J. M.; Morales, J.; Tirado, J. L. *J. Solid State Chem.* **1989**, *82*, 87.

(16) Prokhvatilov, V. G.; Gindin, E. I. *Sov. Phys. Crystallogr.* **1965**, *10*, 191.

(17) Jarosh, D. *Miner. Petrol.* **1987**, *37*, 15

Experimental Section

A series of mixed oxides $Mn_xCo_{3-x}O_4$ with x varying from $x = 1.4$ to $x = 2.0$ in steps of $\Delta x = 0.1$ were synthesized. Mixed Co^{2+} and Mn^{2+} solutions were prepared by dissolving stoichiometric amounts of the corresponding metal chlorides in distilled water. The cations were coprecipitated by slow addition (1 mL min^{-1}) of *n*-butylamine (1 mol L^{-1}), up to $\text{pH} \approx 10.5$. A detailed description of the synthesis procedure has been published elsewhere.^{12,13,18} Some particular compositions ($x = 1.4, 1.5, 1.6, \text{ and } 1.8$) were systematically and cumulatively heated in air between 100 and 1000 °C, kept at each temperature for 5 h, and then quenched to room temperature by rapidly removing them from the furnace. In this paper, a tetragonal phase within the compositional range $1.4 < x < 2.0$ quenched in air will be labelled as **L1**; tetragonal $Mn_xCo_{3-x}O_4$, $2 \leq x \leq 3$ spinels will be hereafter referred as **L2**.

X-ray powder diffraction patterns were recorded at room temperature using a Siemens D-501 diffractometer with monochromatized $\text{Cu K}\alpha$ radiation. Diagrams were recorded in the step scanning mode, with a $0.025^\circ(2\theta)$ step scan and 2 s/step counting time in the range $10^\circ \leq 2\theta \leq 80^\circ$. Divergence slits located in the incident beam were selected to ensure complete illumination of the specimen surface at $12^\circ(2\theta)$. The least-squares structure refinements were undertaken with use of the Rietveld program DBWS-9006PC.¹⁹ Rietveld refinements were made assuming space groups $Fd\bar{3}m$ and $I41/amd$ for cubic and tetragonal spinel-type structures, respectively. For cubic $Fd\bar{3}m$ spinels, 19 parameters were fitted to the 2801 data points: 1 scale factor, 5 background parameters, the zero point for 2θ , 6 profile function parameters (3 for the mixing parameter m and 3 for the fwhm), 1 asymmetry correction parameter (for peaks below $2\theta = 50^\circ$), the cell parameter a , the oxygen positional parameter u , and 3 isotropic thermal parameters B , 1 for each equiposition 8a, 16d, and 32e. For tetragonal $I41/amd$ spinels, the same nonstructural parameters were refined. The structural cell parameters a and c , the oxygen positional parameters $y(O)$ and $z(O)$, and three isotropic thermal parameters B , one for each Wyckoff equipoint (4a, 8d, and 16h), were also refined. Refinements were continued until the parameter shifts were less than 0.3 times the estimated standard deviations. Bond distances for cubic and tetragonal spinel oxides were deduced from a and u , and from a , c , $y(O)$ and $z(O)$, respectively. A quantitative phase analysis has also been undertaken with the Rietveld method. It relies on the relationship²⁰ shown in eq 1:

$$W_p = S_p(ZMV)_p \sum_{i=1}^n S_i(ZMV)_i \quad (1)$$

where W is the relative weight fraction of phase p in a mixture of n phases, and S , Z , M , and V are the Rietveld scale factors, the number of formula units per unit cell, the mass of the formula unit, and the unit-cell volume (\AA^3), respectively. In tetragonal spinels, $a' = \sqrt{2}a$ has been used for convenience.

High-temperature X-ray diffraction studies were carried out using an Anton Paar chamber mounted on a Philips PW 1310 diffractometer. The samples were placed on a platinum strip which also acted as the heating element. The temperature was measured with a Pt-13% Rh/Pt thermocouple welded onto the back of the platinum strip. Differential thermal analysis (DTA) and thermogravimetric (TG) curves were obtained using a Stanton STA 781 simultaneous thermal analyzer. About a 40 mg sample was used, and $\alpha\text{-Al}_2\text{O}_3$ was the inert reference material.

Results and Discussion

X-ray Diffraction Studies. Structural Features.

Figure 1a shows X-ray patterns recorded for samples

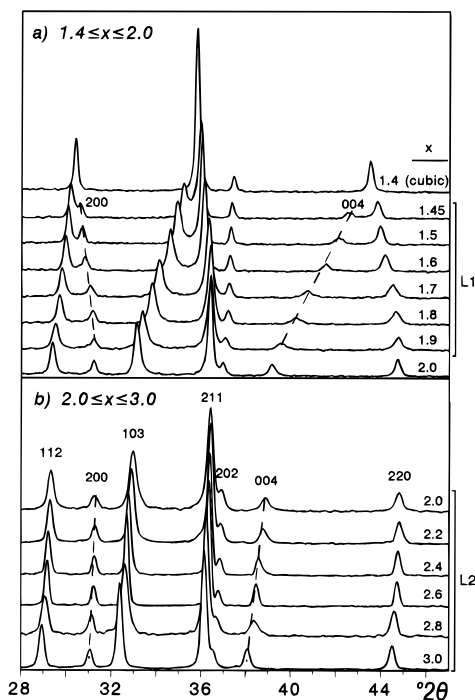


Figure 1. X-ray diffraction patterns of $Mn_xCo_{3-x}O_4$: (a) $1.4 \leq x \leq 2.0$ quenched at 1000 °C; (b) $2.0 \leq x \leq 3.0$ cooled to room temperature. For the sake of clarity, only the $28^\circ \leq 2\theta \leq 47^\circ$ range is presented.

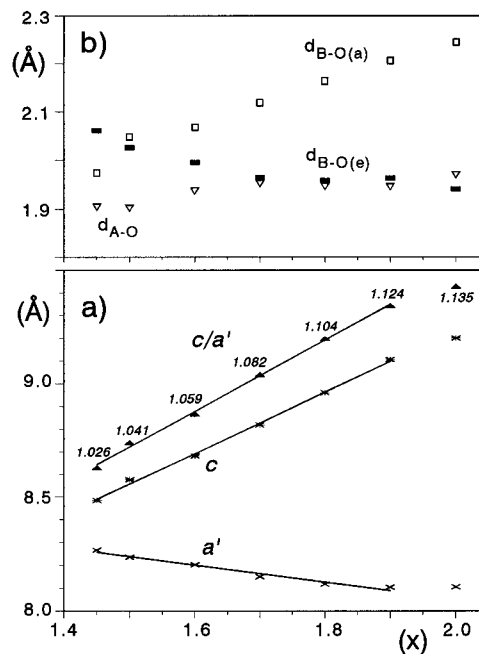


Figure 2. Tetragonal L1 spinel. Variation with composition (x) of (a) a' ($a' = \sqrt{2}a$) and c cell constants, and distortion parameter d' ; (b) tetrahedral d_{A-O} , axial $d_{B-O(a)}$, and equatorial $d_{B-O(e)}$ octahedral bond distances. Data for the composition $x = 2.0$ are included for comparison.

$Mn_xCo_{3-x}O_4$ within the concentration range of the tetragonal **L1** phase ($1.45 \leq x \leq 1.9$), quenched at 1000 °C in air. Patterns corresponding to the cubic $x = 1.4$ and tetragonal $x = 2$ sample quenched at 1000 °C in air are also included for comparison. In Figure 1b diagrams obtained for tetragonal **L2** spinel-type oxides ($2.0 \leq x \leq 3.0$) are presented. In Figure 2a, the variation with composition of the experimental values a' , c , and distortion parameter c/a' for the tetragonal

(18) García-Martínez, O.; Rojas, R. M.; Vila, E.; Martín de Vidales, J. L. *Solid State Ionics* **1993**, *63–65*, 442.

(19) Sakthivel, A.; Young, R. A. *Users Guide to Programs DBWS-9006 and DBWS-9006PC for Rietveld Analysis of X-ray and neutrons Powder Diffraction Patterns*; School of Physics, Georgia Institute of Technology, Atlanta, 1995.

(20) Hill, R. J.; Howard, C. J. *J. Appl. Cryst.* **1987**, *20*, 467.

Table 1. Fractional Atomic Coordinates $y(\text{O})$ and $z(\text{O})$, Tetrahedral and Octahedral (O–O) Bond Distances and O–(A,B)–O Angles Determined for Tetragonal Spinel $\text{Mn}_x\text{Co}_{3-x}\text{O}_4$ ($1.45 \leq x \leq 1.9$). Data for Composition $x = 2.0$ Included for Comparison

	x						
	1.45	1.5	1.6	1.7	1.8	1.9	2.0
oxygen coord							
$y(\text{O})$	–0.497(1)	–0.492(1)	–0.485(1)	–0.4819(9)	–0.482(1)	–0.484(1)	–0.4784(9)
$z(\text{O})$	0.733(1)	0.7389(8)	0.7381(8)	0.7392(7)	0.7413(7)	0.7419(7)	0.7435(7)
O–O octahedra							
d_1 [$\times 2$]	2.892(9)	2.813(9)	2.733(9)	2.670(8)	2.664(9)	2.681(9)	2.618(8)
d_2 [$\times 2$]	2.937(1)	2.9177(7)	2.9075(7)	2.8847(6)	2.8741(5)	2.8690(5)	2.8680(4)
d_3 [$\times 4$]	2.961(9)	2.973(8)	2.989(8)	3.010(7)	3.026(8)	3.050(8)	3.071(8)
d_4 [$\times 4$]	2.744(9)	2.788(8)	2.755(8)	2.766(7)	2.809(7)	2.851(8)	2.861(8)
O–B–O angles							
$\text{O}_e\text{–B–O}_e$ [$\times 2$]	89.1(2)	87.9(2)	86.4(2)	85.6(2)	85.7(2)	86.1(2)	84.8(2)
$\text{O}_e\text{–B–O}_e$ [$\times 2$]	90.9(4)	92.1(4)	93.5(4)	94.4(4)	94.3(4)	93.9(4)	95.2(4)
$\text{O}_a\text{–B–O}_e$ [$\times 4$]	94.5(5)	93.7(4)	94.6(4)	94.8(4)	94.3(4)	93.9(4)	94.1(4)
$\text{O}_a\text{–B–O}_e$ [$\times 4$]	85.6(4)	86.3(4)	85.3(4)	85.2(4)	85.7(4)	86.1(3)	85.9(4)
O–O tetrahedra							
d_5 [$\times 2$]	2.954(9)	3.010(8)	3.068(8)	3.086(7)	3.076(6)	3.050(8)	3.113(8)
d_6 [$\times 4$]	3.191(9)	3.159(8)	3.218(8)	3.247(7)	3.236(6)	3.244(8)	3.217(8)
O–A–O angles							
[$\times 2$]	101.5(2)	104.4(2)	104.4(2)	104.2(2)	104.2(2)	103.0(2)	104.3(2)
[$\times 4$]	113.6(7)	112.1(6)	112.0(5)	112.2(5)	112.5(5)	112.8(5)	112.3(5)

L1 phase, is depicted. Between $x = 1.45$ and 1.9, a linearly decreases from 5.8455(4) to 5.7304(3) Å, while c increases regularly from 8.4843(6) to 9.106(1) Å; the distortion parameter c/a goes from 1.0263(1) to 1.1236(2). Tetragonal **L2** ($2.0 \leq x \leq 3.0$) spinels have cell constants a and c that range from 5.7296(6) to 5.7560(2) Å and from 9.2304(9) to 9.4599(2) Å, respectively, and distortion parameters from 1.1391(3) to 1.1621(1).¹¹

The differences in the variation of the experimental lattice constants of the **L1** and **L2** tetragonal phases are evident from patterns shown in Figure 1. While the **L2** phase has angular positions of reflections (200) and (004) shifting to lower 2θ angles on increasing the manganese content, the tetragonal **L1** phase has the positions of the (200) reflections shifting to higher 2θ angles, and a shift of the (004) reflections to lower 2θ angles than those observed for the **L2** spinel. The variation of the tetragonal cell constant a with composition shows different trends for the **L1** and **L2** tetragonal phases. The compositional limit between **L1** and **L2** solid solutions corresponds to the inflection point of this variation and it is located between $x = 1.9$ and 2.0 (Figure 2a).

If it is assumed that **L2** and quenched **L1** are normal spinels (inversion parameter $\nu = 0$), from $x = 2.0$ the octahedral B-sites in the **L2** tetragonal phase will be fully occupied by $\text{Mn}^{3+}(\text{d}^4)$ cations. Therefore, the manganese incorporated into this phase on going from $x = 2.0$ to 3.0 must be Mn^{2+} located in the tetrahedral A sites. However, in the compositional range of the **L1** phase, the manganese incorporated into the spinel lattice on going from $x = 1.45$ to 1.9 would be Mn^{3+} situated in octahedral B sites. That is why the variation of the distortion parameter c/a is more pronounced for **L1** than for the **L2** compositional range.

In Figure 2b, the variation of the experimental tetrahedral $d_{\text{A–O}}$, axial $d_{\text{B–O(a)}}$ and equatorial $d_{\text{B–O(e)}}$ octahedral bond distances vs composition determined for the **L1** tetragonal spinels, are shown. Structural data as determined from the Rietveld refinement carried out for each composition are summarized in Table 1. In Figure 3, the unit cell of the tetragonal $\text{Mn}_x\text{Co}_{3-x}\text{O}_4$ spinel is illustrated. For the sake of clarity, only

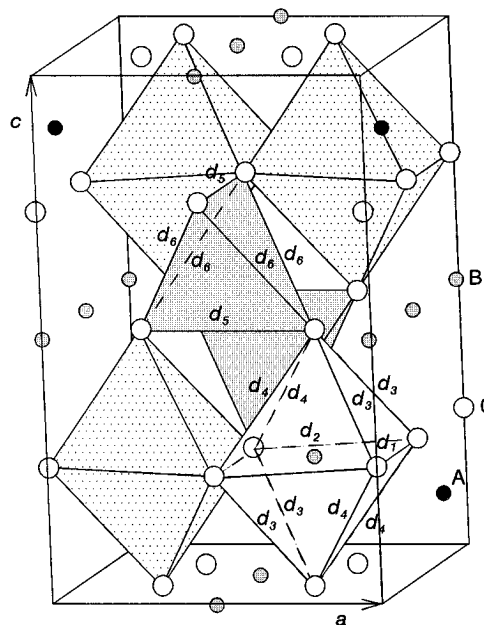


Figure 3. Unit cell of the tetragonal spinel showing the edge-sharing BO_6 octahedra and the AO_4 tetrahedra. Only coordination polyhedra with all atoms within the unit cell are shown. Distances d_1 to d_6 are given in Table 1.

coordination polyhedra with all oxygen atoms enclosed inside the unit cell are shown. The 6-fold coordination polyhedra around the B cations can be regarded as distorted octahedra with four (O–O) distances: d_1 and d_2 in the equatorial plane, and d_3 and d_4 (see Figure 3). The coordination polyhedra around the A cations are elongated tetrahedra with two short d_5 and four long d_6 distances (Table 1).

As is shown in Figure 2b, the axial $d_{\text{B–O(a)}}$ distances increases as the manganese content increases, whereas equatorial $d_{\text{B–O(e)}}$ decreases. For $x = 1.45$, the equatorial distance is longer than the axial bond length. This result is within the variation of the bond distances for $\text{Mn}^{3+}(\text{d}^4)$ in an octahedral environment in tetragonal spinels. The axial $d_{\text{B–O(a)}}$ values are usually longer than the equatorial $d_{\text{B–O(e)}}$ values.^{21,22} For this composition, $x = 1.45$, the coordination polyhedra around B can be

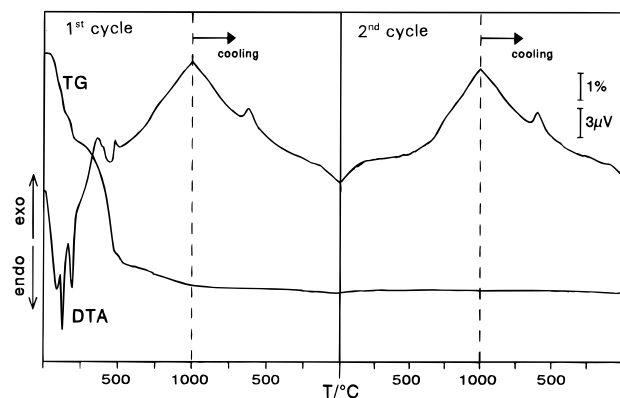


Figure 4. DTA and TG curves recorded for composition $x = 1.8$. Two heating/cooling cycles are presented.

described as a distorted flattened octahedra; whereas from $x = 1.5$ onward the octahedra are elongated along the c axis of the structure (see Table 1).

Thermal Studies. The thermal behavior of $Mn_xCo_{3-x}O_4$ ($1.4 \leq x \leq 1.9$) with temperature has been followed by thermal analysis and high-temperature X-ray diffraction techniques. Samples were also heated to various temperatures and then quenched in air. In Figure 4, DTA and TG curves recorded for sample $x = 1.8$ are presented. The sample was submitted to two consecutive heating/cooling cycles from room temperature to 1000 °C at a 10 °C min⁻¹ heating/cooling rate. In the first heating cycle and between room temperature and ≈ 525 °C, the DTA curve shows a series of thermal effects caused by the removal of water molecules absorbed on the surface of the particles. The experimental mass loss in this temperature range, determined from the TG curve is $\approx 8\%$. Between 525 and 1000 °C the sample experiences another continuous mass loss of $\approx 1\%$ that is not accompanied by any well-defined effect in the DTA curve. This behavior, which has previously been observed in some related systems,¹³ has been assigned to the gradual removal of oxygen, that causes the progressive reduction from Mn^{4+} to Mn^{3+} and from Co^{3+} to Co^{2+} .^{11,23} In the second heating cycle the sample does not experience any mass variation. This result shows that the reduction process only takes place during the first heating cycle and suggests that the cations do not get reoxidized in the subsequent cooling/heating cycles. Cooling DTA traces show an exothermal effect between 650 and 525 °C ($T_{max} = 600$ °C). In the second heating cycle, a broad endothermal effect between 325 and 720 °C is also observed. It was not observed in the first heating cycle due to overlapping of the endothermal effects assigned to dehydration reactions.

Studies of the structural transformations undergone by this sample with temperature were then undertaken by high temperature X-ray diffraction techniques. At room temperature (Figure 5), a mixture of cubic **C** ($x \approx 1.3$) and tetragonal **L2** ($x \approx 2.0$) spinels is observed. From 300 °C onward, the cubic spinel progressively reacts with the tetragonal **L2** spinel; the relative

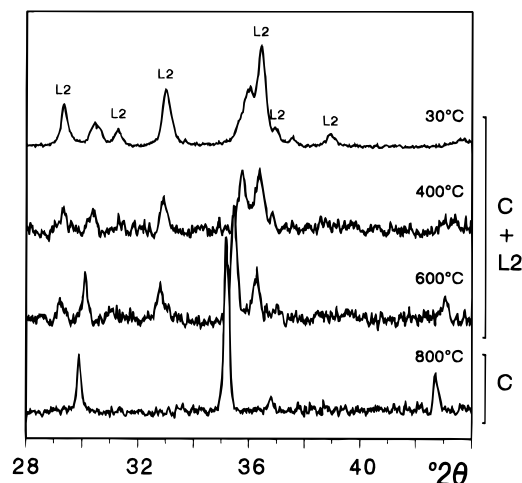


Figure 5. Diffraction patterns recorded for composition $x = 1.8$ in the high-temperature X-ray diffraction chamber (**L2** = tetragonal spinel $Mn_xCo_{3-x}O_4$, $x \approx 2$). Diagrams have been recorded at the temperatures indicated in each pattern.

amount of the former gradually increases at the expense of the latter. This process takes place up to ≈ 725 °C and corresponds to the broad endothermal effect observed between 300–700 °C in the second DTA heating curve (Figure 4). At ≈ 725 °C the tetragonal **L2** spinel disappears and the cubic spinel-type phase $Mn_{1.8}Co_{1.2}O_4$ is formed (Figure 5). During the whole reaction and up to 725 °C, the manganese content of the cubic phase progressively increases up to $x = 1.8$, as shown by the increment of the cubic cell constant; the manganese content of the **L2** phase does not vary. The tetragonal cell parameters of this phase show negligible change as long as the reaction is taking place.

However, when another batch of the initial $x = 1.8$ sample is heated in a furnace at the same temperatures as those in the X-ray chamber and then is quenched in air; some differences are noted, even though the reaction pathway is identical. X-ray diagrams recorded for the sample quenched from 525 to 700 °C (Figure 6) show that, instead of the cubic spinel-type phase, a tetragonal **L1** phase with manganese content identical with that of the corresponding cubic phase is formed (Figure 6). This is because the cubic spinel formed at $T > 500$ °C has a manganese content $x > 1.4$, and it is stable only at high temperature; it cannot be isolated at room temperature but immediately transforms into the tetragonal **L1** phase. The formation of cubic MMn_2O_4 ($M = Co, Zn, Ni, \text{etc.}$) spinels and cubic Mn_3O_4 at high temperature has been reported in the literature;^{24,25} they are observable only by high-temperature X-ray diffraction techniques. In the former case and for $M = Co$, the tetragonal \rightleftharpoons cubic transition takes place at 900 °C,²⁴ while for Mn_3O_4 a reversible phase transition occurs at 1150–1175 °C.²⁵ It follows that the transition temperature increases as the manganese content in the sample increases. For the composition we are dealing with, $x = 1.8$, the cubic spinel is formed as the only phase at $T \approx 725$ °C.

When the sample is cooled within the high-temperature X-ray diffraction chamber, the reverse transformation is observed. Segregation of the tetragonal **L2**

(21) Burns, R. G., *Mineralogical Applications of Crystal Field Theory*, Cambridge University Press: Cambridge, Great Britain, 1970; 224 pp.

(22) West, A. R., *Basic Solid State Chemistry*, John Wiley & Sons: New York, 1984; 415 pp.

(23) Gillot, B. *J. Solid State Chem.* **1994**, *113*, 163.

(24) Irani, K. S.; Sinha, P. B.; Biswas, A. B. *J. Phys. Chem. Solids* **1962**, *23*, 711.

(25) Dorris, S. E.; Mason, T. O. *J. Am. Ceram. Soc.* **1988**, *71*, 379.

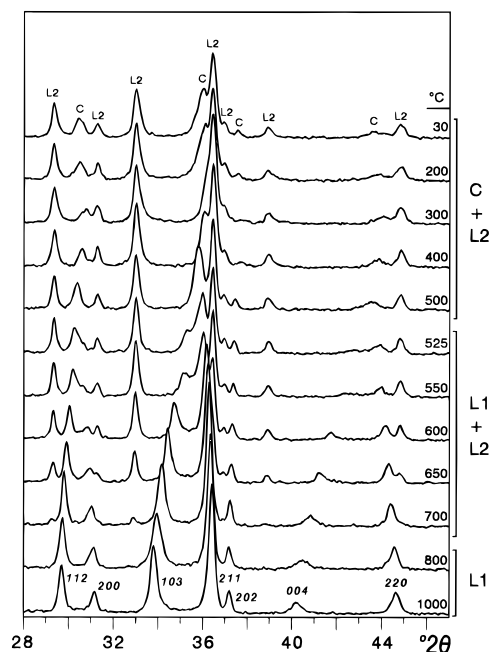


Figure 6. X-ray diffraction patterns for composition $x = 1.8$ quenched from the temperatures indicated in each pattern. (C = cubic spinel, L1 = tetragonal spinel; L2 = tetragonal spinel $Mn_xCo_{3-x}O_4$, $x \approx 2$).

phase takes place, and a mixture of this phase and the cubic $x < 1.8$ spinel is formed. This transformation is also shown in the DTA cooling curves by the presence of a well-defined exothermic effect between 650 and 525 °C ($T_{\max} = 600$ °C). It is caused by the decomposition of the cubic ($x = 1.8$) phase into another cubic spinel with lower manganese content, plus the tetragonal L2 phase. During the cooling process, the cubic structure is retained at temperatures lower than 725 °C and the above-indicated transformation suddenly takes place at ≈ 625 °C.

To study in detail the evolution of the new L1 tetragonal spinels with temperature, batches of each composition ($x = 1.5, 1.6,$ and 1.8) were cumulatively heated from room temperature to 1000 °C, kept at each definite temperature for 5 h and then quenched in air. In Figure 6, X-ray patterns recorded for sample $x = 1.8$ after each thermal treatment are presented. From diagrams shown in Figure 6, the cell parameter values and the percentages of cubic and tetragonal spinels existing at each temperature have been determined. The results are presented in Figure 7a,b, respectively. From these data, the following regions can be distinguished:

(i) From room temperature to 300 °C, the value of the cubic cell constant diminishes and at 300 °C has a minimum value of 8.2241(9) Å; therefore, the Mn/Co ratio in the cubic phase also diminishes (Figure 7a). At the same time, the percentage of the L2 phase increases (Figure 7b) without any significant variation in the lattice constants (Figure 7a).

(ii) From 300 to 500 °C the cubic spinel reacts with the tetragonal L2 spinel. The manganese content of the cubic phase increases progressively, and consequently, the lattice parameter increases (Figure 7a); the percentage of cubic phase in the mixture also increases. Between room temperature and 500 °C the diagrams show a mixture of tetragonal L2 and a cubic spinel-type phase, where the manganese content must be $x \leq 1.4$ (Figure 6).

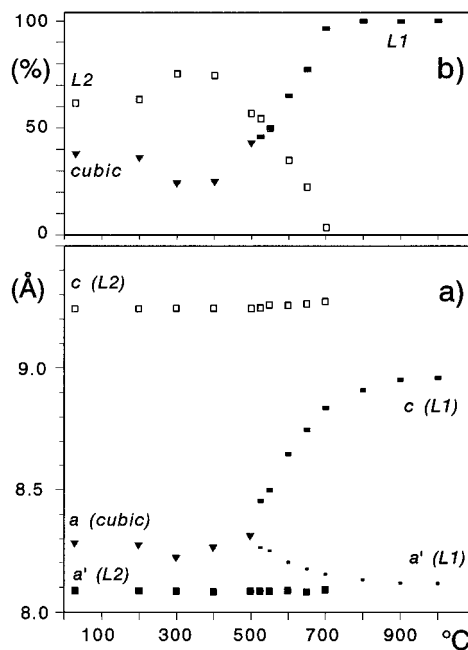


Figure 7. Evolution of (a) cell parameters values; (b) percentages of cubic C, L1 and L2 tetragonal spinels identified for composition $x = 1.8$, quenched at the different temperatures.

(iii) Between 525 and 700 °C the diagrams correspond to a mixture of L1 and L2 tetragonal spinels, the former coming from the cubic high-temperature spinel with $x > 1.4$. As has already been mentioned, tetragonal lattice parameters of the L2 phase do not vary (Figure 7a) but its percentage in the mixture diminishes (Figure 7b).

(iv) Finally, from 800 to 1000 °C tetragonal L1 ($x = 1.8$) is identified in the X-ray patterns as the only phase.

To improve the quality of the X-ray powder patterns, this study has been carried out on specimens previously heated to 1000 °C for 10 h and then slowly cooled within the furnace. Finally, we have also carried out the same study for the cubic spinel $x = 1.4$, which composition corresponds to the limit established by us¹¹ for the $Fd\bar{3}m$ solid solution. At room temperature the cell parameter of this phase is $a = 8.3989(4)$ Å. From 100 to 400 °C, segregation of a tetragonal $I41/amd$ phase is observed. At the same time, the cubic lattice constant decreases and at 300 °C reaches the minimum value 8.2589(4) Å. For 500 °C and higher temperatures a cubic spinel single phase is observed. Samples $x = 1.2$ and 1.3 were also submitted to the same thermal treatment, but in these cases, segregation of the tetragonal L2 phase was not observed.

In general, the existence of cubic spinel-like cobalt manganese oxides can be understood in terms of the concentration of Mn^{3+} ions located in octahedral B sites. If it is low enough (≤ 60 – 65%) the Jahn–Teller distortion is not noticeable and the spinels remain cubic.¹ The location of Mn^{2+} cations in tetrahedral A sites and the allocation of Mn^{3+} and Mn^{4+} in octahedral B-sites in manganite spinels is dramatically influenced by thermal treatments.^{26–28} In our case, the experimental results obtained for the cubic $x = 1.4$ phase can be accounted

(26) McClure, D. S. *J. Phys. Chem. Solids* **1957**, *3*, 311

(27) Navrotsky, A.; Kleppa, O. J. *J. Inorg. Nucl. Chem.* **1967**, *29*, 2701.

(28) O'Neill, H. St.C.; Navrotsky, A. *Am. Miner.* **1983**, *68*, 181

for assuming that in the original cubic spinel, some manganese must be Mn^{2+} located in tetrahedral A sites. On increasing the temperature, it gets oxidized to Mn^{3+} which moves to octahedral B sites, yielding the tetragonal spinel. Therefore, a mixture of cubic ($x < 1.4$) and tetragonal phases is identified between 200 and 400 °C. This behavior is supported by the fact that the oxidation temperature from Mn^{2+} to Mn^{3+} has been reported to be ≈ 280 °C.²³ For 500 °C and higher the reaction between the cubic and tetragonal phases takes place, in the way described above for the sample having $x = 1.8$. It follows that the compositional limit of the cubic manganese cobalt spinel strongly depends on the synthesis procedure and thermal history. In this context, the synthesis conditions (precursors, temperature and time of thermal treatment) are very important,^{8,11,23} and this explains why it is possible to synthesize spinel-type oxides having the same composition but different crystal structures.

Conclusions

The formation of a cubic spinel-type phase in the compositional range $\text{Mn}_x\text{Co}_{3-x}\text{O}_4$ ($1.4 < x < 2.0$) has been achieved. It is formed as a single phase at $T > 500$ °C depending on composition, but it cannot be isolated at room temperature. It readily transforms on quenching into the tetragonal **L1** phase. When the cubic spinel is slowly cooled to room temperature, it decomposes into a mixture of cubic and the tetragonal **L2** phase.

Acknowledgment. The authors thank Mr. J. Berjano for technical assistance with the X-ray powder diffraction. This work was supported by CICyT Project MAT94-0799.

CM950503H